Digital feedback controller for force microscope cantilevers

C. L. Degen, U. Meier, Q. Lin, A. Hunkeler, and B. H. Meier[a)]
Physical Chemistry, ETH Zürich, CH-8093 Zürich, Switzerland

(Received 15 November 2005; accepted 5 February 2006; published online 13 April 2006)

We present a fast, digital signal processor (DSP)-based feedback controller that allows active motion damping of low-k, high-Q cantilevers in magnetic resonance force microscopy. A setup using a piezoelement attached to the cantilever base for actuation and a beam deflection sensor for tip motion detection is employed for controller demonstration. Controller parameters, derived according to stochastic optimal control theory, are formulated in a simple form readily implemented on a DSP, and extensions to other detection and actuation schemes are indicated. The controller is combined with an automated calibration scheme allowing for adaptive parameter adjustment. With the digital device operating at a sampling rate of 625 kHz and 16 bits of dynamic range, we were able to obtain closed-loop quality factors $Q_{\mathrm{cl}}<5$ for cantilevers with $Q\approx 10\,000$ and resonance frequencies up to 15 kHz. This corresponds to an increase in bandwidth of $>10^3$ at undiminished signal to noise, and reduces response time and vibration amplitude by the same factor. © *2006 American Institute of Physics.* [DOI: 10.1063/1.2183221]

I. INTRODUCTION

Fast feedback control of resonating microscale cantilever beams constitutes a crucial component of modern force microscopes. Active control of cantilever vibrations allows to vary the system bandwidth independently, and has, for example, been used to increase acquisition speed of atomic force microscopy (AFM) images or to reduce the force impact on the imaged material (Q control).[1–3]

For applications where maximum force sensitivity is required, such as for measurements of the tiny attraction between spin magnetic moments and a ferromagnetic particle in magnetic resonance force microscopy (MRFM), cantilevers with low spring constants and high quality factors must be employed.[4–7] The same properties are, however, connected to large oscillation amplitudes, small system bandwidths, and long response times, all of which are prohibitive for a precise, stable, and reasonably fast operation. Furthermore, thermal motions of the cantilever—when uncontrolled—limit the spatial resolution well above the atomic scale. It has been shown that in this situation, active feedback allows to eliminate all these drawbacks without significantly affecting the signal-to-noise ratio of the force measurement,[8,9] enabling to reach all goals simultaneously.

Feedback controllers can be realized in several different ways. For frequency modulated AFM, analog and digital implementations based on a phase-locked loop have been presented.[1,10] Here we consider the slightly different problem of a cantilever driven by the signal force itself and the task is to reduce the amplitude of the induced vibrations. Due to the low spring constant of the cantilevers, the controller must consider not only the effect of the external force but also the random thermal motions of the cantilever.[8,9]

In this contribution we present an accurate, versatile digital feedback controller based on a digital signal processor (DSP) for active feedback damping of vibrating cantilevers. The use of a DSP eliminates many disadvantages of analog implementations, such as start-up delays, temperature drifts, aging, limited reproducibility, and low flexibility.[11] Furthermore, digital controllers are well suited for remote operation that can be combined with automated calibration schemes for adaptive control. On the other hand, the lack of fast DSP's and accurate, high-speed analog-digital converters have in the past prevented a wider application of digital controllers. In this respect, MRFM is not very demanding due to the relatively low oscillator frequencies involved (typically <10 kHz), compared to the stiff, high frequency cantilevers (10–1000 kHz) widely used in standard AFM. The application of a DSP-based feedback controller in the context of MRFM has indeed been described recently.[12]

Our instrument is designed for systems where cantilever motions are controlled through base shifts using a piezoactuator.[13] Base piezoactuation benefits from simple technical realization, is easy to calibrate, and can be used with any cantilever. For motion detection, we consider a beam deflection sensor where the excursion of the cantilever tip is measured indirectly by the bending of the beam.[14] It is clear that controller dynamics will be affected when using different actuation and detection schemes. Nevertheless, controller characteristics are expected to be the same, and merely the actual parameters must be modified for different implementations. Following the work of Garbini *et al.*,[8] we give a derivation of the stochastic optimal controller that applies for our implementation, and provide analytical expressions that can be generalized to other actuation/detection combinations.

a)Electronic mail: beme@ethz.ch

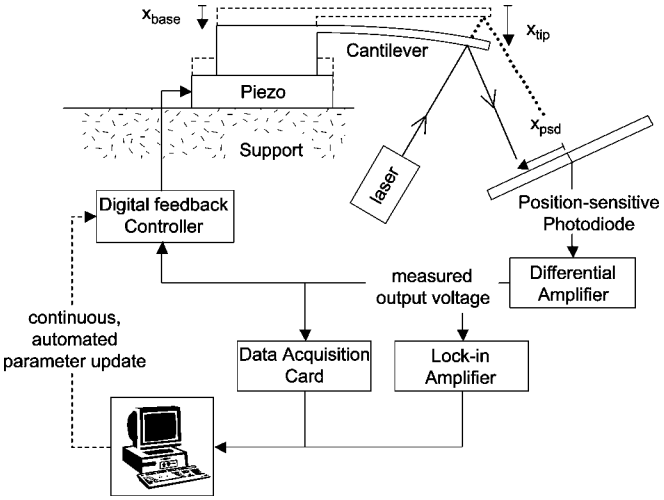

FIG. 1. Experimental setup. The dashed shape shows the cantilever position in rest and displays the role of x_{tip}, x_{base}, and x_{PSD}.

II. THEORY

A. System

The response of the cantilever to a small force f acting on the tip can be described in terms of a damped harmonic oscillator with the associated Laplace transfer function,

$$G(s)=\frac{X_{\mathrm{tip}}(s)}{F(s)/k}=\frac{\omega_n^2}{s^2+s(\omega_n/Q)+\omega_n^2}, \tag{1}$$

where x_{tip} is the position of the cantilever tip, $\omega_n=\sqrt{k/m}$ the natural frequency, $Q=\sqrt{km}/b$ the quality factor, k the spring constant, m the effective mass, and b the friction.

Tip response to small control displacements of the base x_{base} is governed by[8]

$$G_a(s)=\frac{X_{\mathrm{tip}}(s)}{X_{\mathrm{base}}(s)}=\frac{s(\omega_n/Q)+\omega_n^2}{s^2+s(\omega_n/Q)+\omega_n^2}, \tag{2}$$

i.e., the control dynamics of tip and base actutation are generally not the same.[15]

Motions are detected by an optical deflection sensor that measures cantilever bending by the shift of a reflected laser beam captured by a position sensitive (quadrant) photodiode[14] (PSD) (cf. Fig. 1). The shift of the laser spot on the PSD is given by $x_{\mathrm{PSD}}=x_{\mathrm{tip}}-x_{\mathrm{base}}$, omitting the deflective amplification factor,[16] with the associated transfer function,

$$G_b(s)=\frac{X_{\mathrm{PSD}}(s)}{X_{\mathrm{base}}(s)}=G_a(s)-1. \tag{3}$$

Notice that measured quantity (x_{PSD}) and controlled quantity (x_{tip}) are not the same.

Consequently, the respective closed-loop response of x_{tip} and x_{PSD} to a force acting on the cantilever tip (i.e., the force signal) is given by

$$G_{\mathrm{cl}}^{\mathrm{tip}}(s)=\frac{X_{\mathrm{tip}}(s)}{F(s)/k}=\frac{G(s)}{1+G_a(s)\{H(s)/[1+H(s)]\}} \tag{4}$$

and

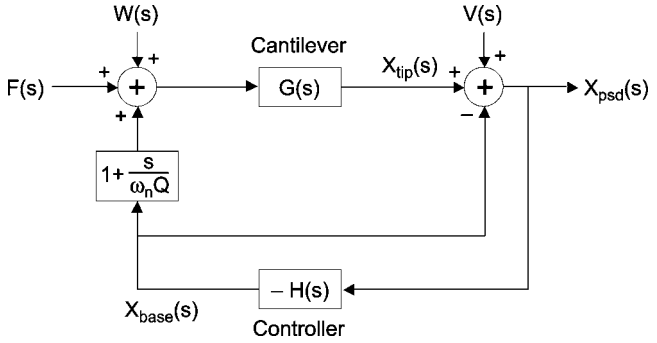

FIG. 2. Schematic representation of the control system.

$$G_{\mathrm{cl}}(s)=\frac{X_{\mathrm{PSD}}(s)}{F(s)/k}=\frac{G(s)}{1+G_b(s)H(s)}, \tag{5}$$

where $H\equiv X_{\mathrm{base}}/X_{\mathrm{PSD}}$ is the controller transfer function.

Noise is modeled by a process force noise component $w(t)$ (in general Brownian noise) and a measurement displacement noise component $v(t)$ (predominantly photodiode shot noise), as shown in Fig. 2.[5,16] Noise is always assumed to be white and uncorrelated, $\langle w(t)w(t')\rangle=\langle v(t)v(t')\rangle=\delta(t-t')$ and $\langle w(t)v(t)\rangle=0$, respectively. Other noise sources, though present, are neglected for the derivation of the controller but will be mentioned below. We can further attribute power spectral densities S_w and S_v to $w(t)$ and $v(t)$, respectively, in order to obtain expressions for the open- and closed-loop photodiode output signal in the presence of noise,

$$S_{\mathrm{op}}(s)=|G(s)|^2(S_w+S_f)+S_v, \tag{6}$$

$$S_{\mathrm{cl}}(s)=\frac{|G(s)|^2(S_w+S_f)+S_v}{|1+G_b(s)H(s)|^2}, \tag{7}$$

where S_f is the spectral density of the external force $f(t)$, i.e., the quantity of interest. $S_{\mathrm{op}}(s)$ and $S_{\mathrm{cl}}(s)$ are used to determine cantilever parameters experimentally (see below).

B. Optimal controller

Because the noise sources for this problem are well known, stochastic optimal control theory can be used to tailor a controller response $H_{\mathrm{oc}}(s)$ that gives optimal performance. $H_{\mathrm{oc}}(s)$ has itself the form of a harmonic oscillator,[8]

$$H_{\mathrm{oc}}(s)=\frac{X_{\mathrm{base}}(s)}{X_{\mathrm{PSD}}(s)}=\frac{K_{\mathrm{oc}}(s+z_{\mathrm{oc}})}{s^2+s(\omega_{\mathrm{oc}}/Q_{\mathrm{oc}})+\omega_{\mathrm{oc}}^2}, \tag{8}$$

where parameters K_{oc}, z_{oc}, ω_{oc}, and Q_{oc} depend on cantilever characteristics and control power. A separate derivation (see Appendix) shows that the particular case where beam deflection is used for detection and base shifts for actuation requires different parameter values than, e.g., an interferometer detection,[8]

$$K_{\mathrm{oc}}=\frac{1}{2}\omega_n\alpha\beta\frac{2/Q(1+\alpha^2/2)+(1-\alpha/Q)(\alpha+\beta+2/Q)}{1-\alpha/Q}, \tag{9}$$

$$z_{\mathrm{oc}} = \frac{1}{2}\omega_n \frac{(\alpha + 4/Q - 2\alpha/Q^2)(\beta + 2/Q) - 4(1 - \alpha/Q)}{(\alpha + \beta + 2/Q)(1 - \alpha/Q) + 2/Q(1 + \alpha^2/2)}, \tag{10}$$

$$\omega_{\mathrm{oc}} = \omega_n \sqrt{\frac{(1 + \alpha^2/2)(1 + \beta/Q + \beta^2/2)}{1 - \alpha/Q}}, \tag{11}$$

$$Q_{\mathrm{oc}} = \frac{\sqrt{(1 - \alpha/Q)(1 + \alpha^2/2)(1 + \beta/Q + \beta^2/2)}}{(\alpha + \beta + 1/Q) + (1/2)\alpha\beta(\alpha + \beta + 2/Q) - \alpha^2/Q(1/2 + \beta/Q + \beta^2/2)}, \tag{12}$$

where

$$\alpha = \sqrt{\frac{\zeta_c^2}{Q^2} + 2\zeta_c - 2} - \frac{\zeta_c}{Q} \text{ and } \zeta_c^2 = 1 + \frac{\sigma_{x,\mathrm{tip}}^2}{\sigma_{x,\mathrm{base}}^2}, \tag{13}$$

$$\beta = \sqrt{\frac{1}{Q^2} + 2\zeta_o - 2} - \frac{1}{Q} \text{ and } \zeta_o^2 = 1 + \frac{S_w}{S_v}, \tag{14}$$

respectively. $\sigma_{x,\mathrm{tip}}^2/\sigma_{x,\mathrm{base}}^2$ denote the ratio of the variances of tip and base excursions, and S_w/S_v the ratio of respective excitation and measurement noise spectral densities. The values of α and β thus reflect how much control and input filtering is applied, respectively.

In practice, the controller parameters (9)–(12) are calculated on the basis of experimentally determined values of ω_n, Q, and S_w/S_v that can be determined, e.g., by fitting the open loop noise spectral density of the cantilever $S_{\mathrm{op}}(s)$. The fourth quantity, the ratio $\sigma_{x,\mathrm{tip}}^2/\sigma_{x,\mathrm{base}}^2$, is left as a free parameter to reach the desired level of feedback damping. Alternatively, it is often more convenient to express the amount of feedback by the closed-loop quality factor Q_{cl}, which determines α according to

$$\alpha = \frac{Q}{Q_{\mathrm{cl}}}[\sqrt{\zeta^4 + 2/Q^2} - \zeta^2]^{1/2} - Q[\sqrt{\zeta^4 + 2/Q^2} - \zeta^2], \tag{15}$$

where $\zeta^2 = 1 - 1/(2Q_{\mathrm{cl}}^2)$.

C. Digital controller

A digital controller is conventionally described by the z-transform response function forming the discrete time equivalent to the Laplace transform used for time-continuous systems.[17,18] Through the strict correspondence between a z function $H(z)$ and its Laplace equivalent $H(s)$—that is, they are originating from the same time domain function—the former can be easily derived.[18,19]

The z function of the controller depends on the details of the sampling process. We use zero-order-hold (zoh) sampling,[17,18] where the appropriate z function is given by $H^{(\mathrm{zoh})}(z) = (1 - z^{-1})\mathcal{Z}[H(s)/s]$. Here, $\mathcal{Z}$ indicates the z correspondent of the enclosed Laplace function. Applying this relation to the optimal controller $H_{\mathrm{oc}}(s)$, the desired z function is found to be

$$H_{\mathrm{oc}}(z) = \frac{b_0 + b_1 z^{-1} + b_2 z^{-2}}{1 - a_1 z^{-1} - a_2 z^{-2}}, \tag{16}$$

where

$$a_1 = 2e^{-aT}\cos\omega T, \tag{17}$$

$$a_2 = -e^{-2aT}, \tag{18}$$

$$b_0 = 0, \tag{19}$$

$$b_1 = \frac{K_{\mathrm{oc}}}{\omega}\left[\frac{z_{\mathrm{oc}}\omega}{\omega_{\mathrm{oc}}^2}(1 - e^{-aT}\cos\omega T) + \left(1 - \frac{z_{\mathrm{oc}}a}{\omega_{\mathrm{oc}}^2}\right)e^{-aT}\sin\omega T\right], \tag{20}$$

$$b_2 = \frac{K_{\mathrm{oc}}}{\omega}\left[\frac{z_{\mathrm{oc}}\omega}{\omega_{\mathrm{oc}}^2}(e^{-2aT} - e^{-aT}\cos\omega T) - \left(1 - \frac{z_{\mathrm{oc}}a}{\omega_{\mathrm{oc}}^2}\right)e^{-aT}\sin\omega T\right]. \tag{21}$$

Here, T is the clock sampling time, $a = \omega_{\mathrm{oc}}/2Q$ the inverse ring-down time, and $\omega^2 = \omega_{\mathrm{oc}}^2 - a^2$ the (damped) controller resonance frequency. The implementation of the controller on a digital signal processor based on these coefficients is straightforward and depicted in the block diagram in Fig. 3(a).

Digital controllers require a finite time for computation of the output signal. The delay of the response can lead to unwanted effects and deteriorate the performance of the controller. A direct consequence of a time lag are phase shifts in the frequency response that grow linearly with frequency and effectively limit the bandwidth of the device. It is therefore often beneficial to include a digital compensating element in the controller response function that corrects the phase distortion.[20] Noticing that a time delay has a Laplace response $e^{-\tau s}$, a particularly simple choice for a compensator is $(1 + \tau s)$ that corrects the phase shift to first order in τs. Adding this compensator to the controller $H_{\mathrm{oc}}(s)$ results in

$$H_{\mathrm{oc}}^{\mathrm{c}}(s) = \frac{K_{\mathrm{oc}}(s + z_{\mathrm{oc}})(1 + \tau s)}{s^2 + (\omega_{\mathrm{oc}}/Q_{\mathrm{oc}})s + \omega_{\mathrm{oc}}^2}. \tag{22}$$

Note that although $(1 + \tau s)$ does not conserve amplitude and even though more sophisticated compensators are available[20] the simple form allows us to use the same z-transfer function (16) without requiring additional higher order coefficients ($n > 2$), which would in turn increase the delay. The modified $a_n^{\mathrm{c}}, b_n^{\mathrm{c}}$ for the compensated controller become

$$a_1^{\mathrm{c}} = a_1, \tag{23}$$

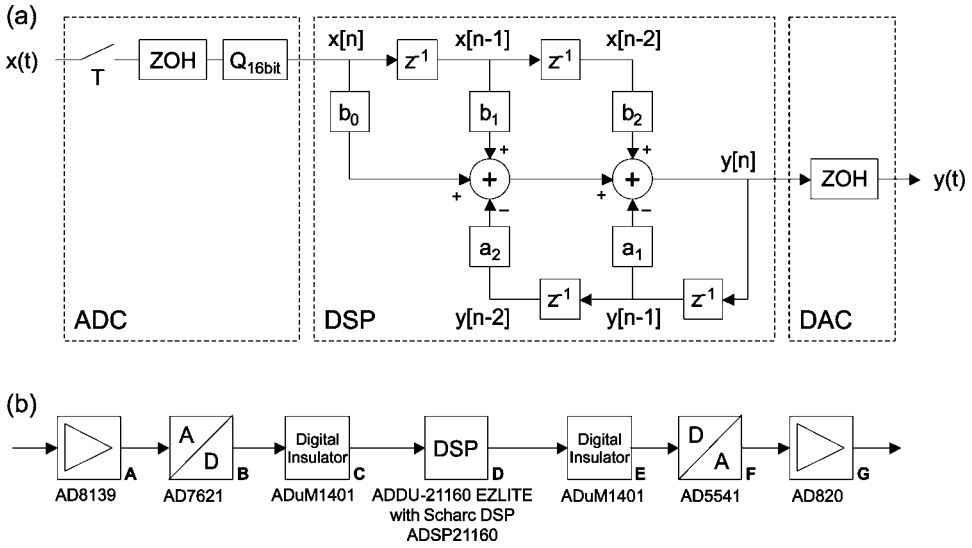

FIG. 3. (a) Block diagram of the computation flow in the digital controller. Quadratic boxes represent either multiplications by a parameter or a register shift, i.e., a unit time delay T. A new output value is calculated according to $y[n]=b_0x[n]+b_1x[n-1]+b_2x[n-2]-a_1y[n-1]-a_2y[n-2]$ on the basis of the last few input and output values $x[n-i]$, $y[n-i]$, respectively. See, e.g., Ref. 17 for further details. (b) Interconnection scheme. The input side consists of an amplifier/filter stage (A), the A/D converter (B), and a galvanic isolation (C). On the output side [(E)–(G)] similar elements are used in reverse order. A/D and D/A converters have an analog range of 5 V at 16 bit digital resolution and are clocked by the DSP(D) at 625 kS/s. The DSP operates at a core clock speed of 80 MHz and uses a 32 bit floating-point arithematic. Communication with the DSP was enabled over USB (for programming) and RS-232 (for controller parameter update during measurements), respectively. A typical controller parameter update required ~100 ms. All elements [(A)–(G)] are availabe from Analog Devices Inc.

$$a_2^c = a_2, \tag{24}$$

$$b_0^c = \tau K_{oc} \tag{25}$$

$$b_1^c = b_1 + \tau\frac{K_{oc}}{\omega}[(z_{oc}-a)e^{-aT}\sin\omega T - \omega(e^{-aT}\cos\omega T + 1)], \tag{26}$$

$$b_2^c = b_2 - \tau\frac{K_{oc}}{\omega}[(z_{oc}-a)e^{-aT}\sin\omega T - \omega e^{-aT}\cos\omega T]. \tag{27}$$

As a final remark we note that the operation principle of a digital controller represented by a transfer function of the form of Eq. (16) is very flexible. Provided bandwidth and dynamic range of the digital circuit are sufficient, virtually any (single-input/single-output) process can be controlled by the instrument by simply choosing different values for the coefficients a_n, b_n.

III. IMPLEMENTATION

A. Controller

The implementation of the controller is depicted in Fig. 3(b). A combination of 16 bit digital resolution and 625 kS/s sampling speed is chosen, capable of handling ~96 dB of dynamic range at a predicted bandwidth of >10 kHz (Ref. 21). In order to suppress noise, analog and digital circuit are electrically isolated, and separate power supplies are used for analog to digital (A/D) and digital to analog (D/A) converters and the DSP, respectively. Computation required 3.5 clock cycles (5.6 μs). The effective input/output delay time was $\tau \sim 7.5$ μs (see Fig. 4). The bandwidth of our implementation is limited by the maximum sampling rate of the D/A converter, and could be increased by employing faster converters or a parallel arrangement, possibly at the cost of a lower dynamic range.

B. Cantilever system

Controller performance was demonstrated on a home-built probe assembly[22] sketched in Fig. 1. Commercially available silicon-nitride cantilevers (Veeco Inc.) with spring constants $k=0.01-0.5$ N/m and resonance frequencies $\omega/2\pi=0.4-40$ kHz (lower frequencies accessed by tip loading) were employed. An $\approx 3\times 2\times 1$ mm^3 sized piezoactuator

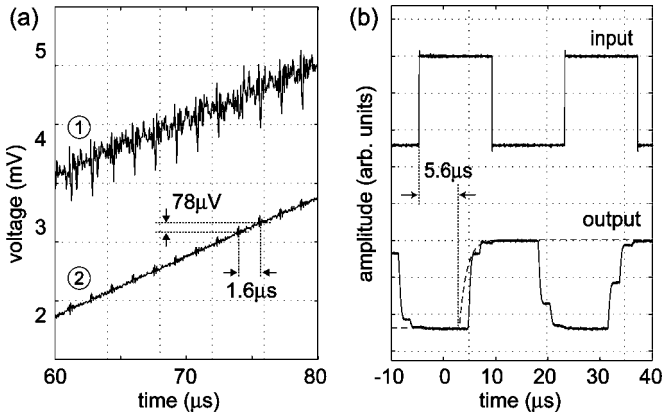

FIG. 4. (a) Cutaway of a sawtooth wave form generated by the DSP and measured in 20 MHz (1) and 50 kHz (2) bandwidths, respectively. Voltage resolution is 78 μV and sampling time per data point is 1.6 μs. (b) Computation delay made visible by connecting a 50 kHz square wave signal to the controller input (upper curve), producing the output shown below. The delay equals in average 4 (=3.5+0.5) clock cycles ~6.4 μs. Taking input filter (160 kHz, dashed line) into account results in effective delay time of ~7.5 μs. The same value is obtained from phase response analysis (see Fig. 5).

(Staveley NDT Technologies) with 235 pF capacitance and 420 pm/V transductance served for base control. A linear expansion characteristic neglecting hysteresis or creep effects is assumed. Actuation voltages for thermal noise damping were typically around 10 mV_{rms} when substantial control was applied.

C. Automated calibration protocol

The digital controller can be combined with an automated calibration protocol, which allows for a self-acting update of controller parameters. Our calibration scheme involved the following steps.

(1) Controller output is disabled.
(2) Cantilever parameters ω_n, Q and the noise ratio S_w/S_v are determined by noise analysis, e.g, by fitting the open loop spectral density of the photodiode $S_{op}(s)$ [Eq. (6)] or using similar techniques.[23,24]
(3) Controller parameters a_n, b_n are calculated according to Eqs. (9)–(12), (15), (14), and (23)–(27). In addition to ω_n, Q, and S_w/S_v, the following parameters are required: a desired closed loop quality Q_{cl}, the controller computation delay τ, and the sampling time T.
(4) The DSP is updated and output enabled.
(5) Step 2 is repeated to characterize/verify the correct closed-loop behavior.

IV. PERFORMANCE TESTS

In a first step dynamic range and timing resolution of the controller were examined. The digital resolution was demonstrated by generating a sawtooth wave form by the DSP and recording the analog output as depicted in Fig. 4(a). The least significant bit corresponds to an analog resolution of 78 μV. Timing characteristics are evaluated in Fig. 4(b), where the input of the controller operating in feedthrough mode [i.e., all coefficients in Eq. (16) are zero except $b_0=1$] is connected to a square wave.

Next it was verified that the controller reproduces the desired transfer characteristics. In Fig. 5 the theoretical response function $H_{oc}(s)$ [Eq. (8)] is compared to the experimentally measured controller response based on the parameters $\{a_n, b_n\}$ associated with $H_{oc}(s)$. While the agreement of the amplitude response is virtually perfect, the linearly growing phase deviation associated with the computation delay can be observed in the phase response. Repeating the measurement using the delay compensated parameters $\{a_n^c, b_n^c\}$ shows that the phase distortion can be efficiently reduced in the desired frequency range.

To demonstrate feedback control of the cantilever, the controller output was connected to the piezobase actuator of the AFM and the photodiode signal was fed into the controller input. Two aspects were considered: the damping of thermal cantilever motions, and the dynamic behavior when an external driving force—that is, a signal—is present.

Figure 6 depicts a representative experiment where the controller was used to damp the thermal motions of the cantilever. Part (a) shows the measured open-loop noise spectral density together with a fit to S_{op} [Eq. (6)]. An additional $1/f$ measurement noise component, attributed to fluctuations in the laser beam intensity, was included for fitting. Part (b) depicts the result of a second measurement after enabling DSP output using the appropriate controller parameters as given in the caption. Notice that in contrast to (a), the closed-loop spectral density S_{cl} (solid line) in (b) was calculated entirely from cantilever parameters and contains no adjustable parameters, thus the theoretical model is confirmed rather accurately.

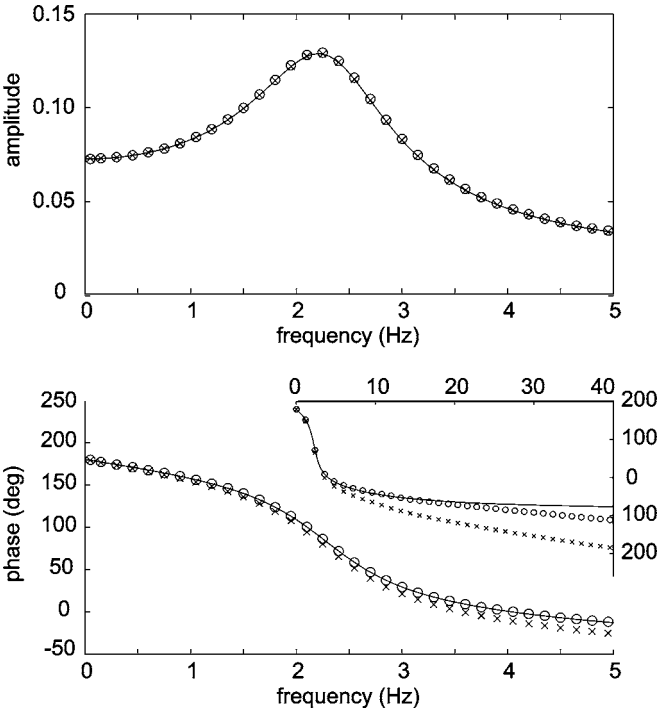

FIG. 5. Transfer function of the controller based using the set of parameters given in the caption of Fig. 6. Experimental amplitude and phase response (crosses) were recorded with a lock-in amplifier. The solid line shows the theoretically calculated transfer function $H_{oc}(s)$. Including a delay compensator significantly improves phase response (circles). Uncompensated, the phase at 5 kHz lags already 13.5° behind, while the deviation stays below 10° up to 21.6 kHz, when the phase is corrected (inset).

Damping of thermal noise was examined using several different cantilevers with resonance frequencies ranging between 0.4 and 40 kHz. Below 15 kHz, an arbitrary level of damping could be applied without observing any deviations from the theoretically predicted behavior. Higher frequencies were still controllable for moderate effort ($Q_{cl} \sim 50$ at 40 kHz) but showed distortions if control was further raised. This is in agreement with sample rate selection rules[21] that recommend a bandwidth of $>30\times$ the relevant system frequency, making our instrument applicable for resonance frequencies up to $\sim$10 kHz. Furthermore, additional checks with low friction cantilevers ($Q \sim 100\,000$, cantilever spring constant of 0.8 mN/m) suggest that the controller is compatible with higher quality factors and lower spring constants.

In a last step, the dynamic properties of the controlled and uncontrolled cantilevers were investigated. For this purpose an external force was applied to the tip, and switched on and off in fixed intervals. Forces on the tip loaded cantilever were generated via inductive coupling from a nearby solenoid coil connected to an amplitude modulated radio-frequency source.

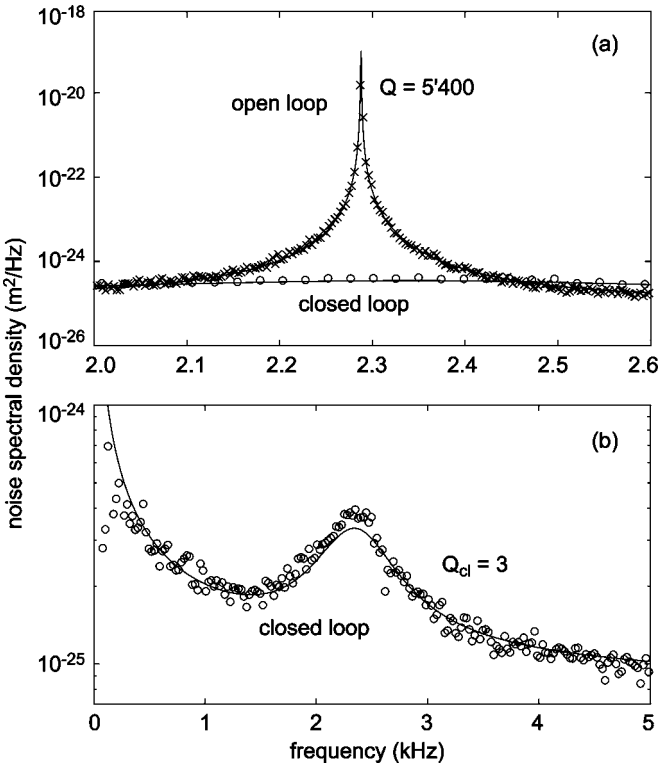

FIG. 6. Thermal noise spectral densities of the (a) uncontrolled and (b) controlled cantilevers. Experimental data are given as crosses (no feedback) and circles (with feedback), respectively. The solid line in (a) represents a least-squares fit of S_{op} to the experimental data, while in (b) it depicts the calculated spectral density S_{cl} without any free fit parameter. Relevant experimental parameters were $f_n=2287.84$ Hz, $Q=5400$, and $k=20$ mN/m for the cantilever, $\zeta_e=0.0431$ ($\beta=0.206$) for the noise ratio, and $\zeta_c=0.121$ ($\alpha=0.342$) for the control ratio. This gives the following controller parameters: $K_{\mathrm{oc}}=279.4$ rad/s, $z_{\mathrm{oc}}=-5.139\times10^4$ rad/s, $\omega_{\mathrm{oc}}=14.95\times10^4$ rad/s, and $Q_{\mathrm{oc}}=1.828$.

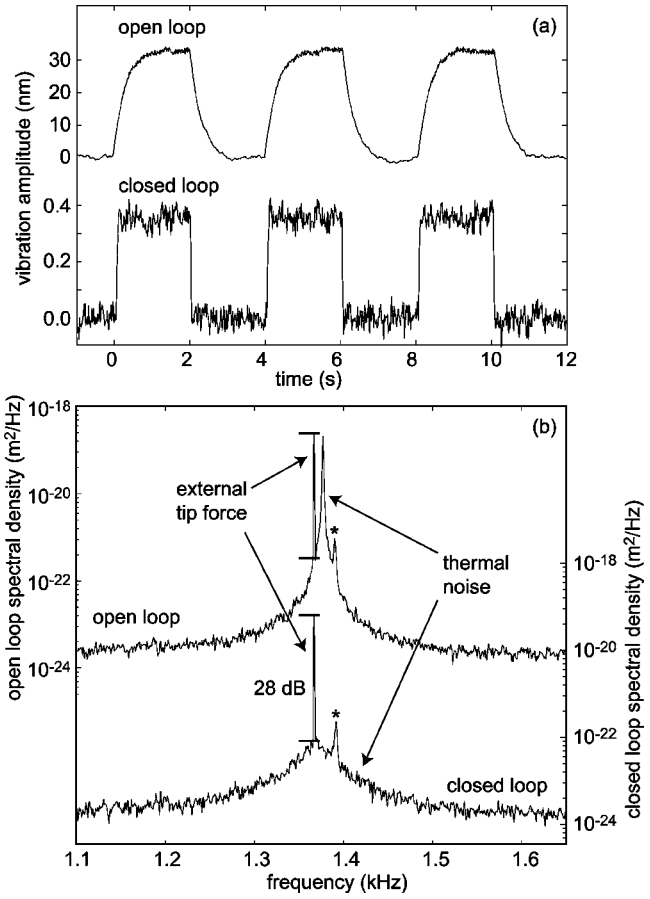

FIG. 7. (a) Dynamic response of the open- and closed-loop systems to an external tip force applied on-resonance ($f_n=1377$ Hz), measured by a lock-in amplifier with time constant $\tau\sim\tau_{\mathrm{cl}}$. Bandwidth is enhanced by the ratio of the quality factors $Q=3000$ and $Q_{\mathrm{cl}}=35$, respectively, while vibrations and response times are scaled down by the same amount. Note that the ratio between the two amplitude scales is Q/Q_{cl}. (b) Corresponding spectral density plots. The force was applied 15 Hz below f_n for better visibility. Signal-to-noise ratio is ~28 dB, and unaffected by feedback control. The peak marked by an asterisk stem from residual mechanical vibrations present in the experimental setup.

The result is shown in Fig. 7(a). The increase of system bandwidth ($=Q/Q_{\mathrm{cl}}\sim87$) upon feedback damping can be manifested in two respects. First, the controlled system reacts almost instantaneously to the external force with a response time $\tau_{\mathrm{cl}}=2Q_{\mathrm{cl}}/\omega_n\sim8$ ms, while the uncontrolled cantilever requires $\tau_{\mathrm{op}}=2Q/\omega_n\sim0.7$ s to build up oscillations. Second, tip excursions are reduced by the same factor. This reduction also applies to thermal vibrations, although this is not directly obvious from Fig. 7(a). Due to the very narrow bandwidth of the open-loop system, measurement noise is dominated by contributions from the vicinity of the cantilever resonance frequency. For the closed loop system, however, a wide range of frequencies must be taken into account, and a much higher relative noise level results. In essence, this means that the fast response time of the controlled system comes at the cost of increased noise. For measurements exceeding the response time τ_{op}, i.e., when the measurement bandwidth is made smaller than the bandwidth of the uncontrolled cantilever, the signal-to-noise ratio of the closed-loop system approaches that of the open-loop system. This is indicated in Fig. 7(b), depicting the power spectral densities from the previous figure (Fig. 6). The external signal, visible as a separate peak, has a reserve of 28 dB on the noise level irrespective of feedback control. Moreover, the signal-to-noise is not affected by working off-resonance, because thermal noise and force signal are subject to the same frequency response [Eq. (6)]. Notice, however, that both findings are only valid as long as cantilever thermal noise is substantially larger than the noise of the position sensor, otherwise the signal-to-noise is degraded indeed.

V. DISCUSSION

A fast, high-resolution digital feedback controller for motion damping of low-k, high-Q cantilevers has been constructed. The controller operates at a sampling rate of 625 kHz combined with fully resolved 16 bits (96 dB) of analog/digital dynamic range. Computation delay is on the order of ~7 μs and digitally compensated for cantilever resonance frequencies up to 20 kHz. Performance evaluation showed that (i) the controller reproduces the theoretical response, (ii) thermal motions of cantilevers can be efficiently damped down to the optical detection limit, reaching closed-loop quality factors in the order of $Q_{\mathrm{cl}}=3$, and (iii) the signal-to-noise ratio of an external force signal is unaffected by the feedback.

Parameters characterizing controller dynamics have been derived according to stochastic optimal control. The parameters are specific for the present cantilever system—where base shifts through a piezoelement and laser beam deflection are used for actuation and detection, respectively—but are easily extended to other setups. Expressions that connect these parameters to the coefficients of the digital controller were provided and can be readily implemented on most DSP's. An automated calibration scheme for adaptive parameter adjustment was presented. Further progress in microelectronics will allow to implement digital controllers operating at a much higher rates, in particular, with regard to high frequency mechanical oscillators employed routinely in atomic force microscopy.

ACKNOWLEDGMENTS

The authors thank G. Moresi and A. Trabesinger for stimulating discussions. Financial support of the ETH Zurich, the Schweizerischer Nationalfonds (SNF), and the Kommission für Technologie und Innovation (KTI) is gratefully acknowledged.

APPENDIX: CONTROLLER DERIVATION

This Appendix gives a compact derivation of the steady-state optimal feedback controller for a base-actuated cantilever with beam deflection motion detection, in order to provide K_{oc}, z_{oc}, ω_{oc}, and Q_{oc} [Eqs. (9)–(12)]. We follow the procedure and notation outlined by Garbini *et al.*[8] and refer to Refs. 25 and 26 for further details.

Consider the steady-state system,

$$\dot{\mathbf{x}}(t) = \mathbf{A}\mathbf{x}(t) + \mathbf{B}\mathbf{u}(t) + \mathbf{G}\mathbf{w}(t), \tag{A1}$$

$$\mathbf{y}(t) = \mathbf{C}\mathbf{x}(t) + \mathbf{D}\mathbf{u}(t) + \mathbf{v}(t), \tag{A2}$$

where $\mathbf{x}(t)$ is the state variable subjected to control, $\mathbf{y}(t)$ the observed variable, and $\mathbf{u}(t)$ the control variable. $\mathbf{w}(t)$ and $\mathbf{v}(t)$ denote white and uncorrelated excitation and measurement noise processes.

For the specific case of a base actuated cantilever with deflection detection,

$$u(t) = x_{\text{base}}(t) + \dot{x}_{\text{base}}(t)/(\omega_n Q), \tag{A3}$$

$$y(t) = x_{\text{tip}}(t) - x_{\text{base}}(t), \tag{A4}$$

thus (A1) and (A2) are explicitly

$$\begin{pmatrix} \dot{v}'_{\text{tip}} \\ \dot{x}_{\text{tip}} \end{pmatrix} = \begin{pmatrix} -\omega_n/Q & -\omega_n^2 \\ 1 & 0 \end{pmatrix} \begin{pmatrix} v'_{\text{tip}} \\ x_{\text{tip}} \end{pmatrix} + \begin{pmatrix} \omega_n^2 - \omega_n^2/Q^2 \\ \omega_n/Q \end{pmatrix} x_{\text{base}}(t) + \begin{pmatrix} \omega_n^2 \\ 0 \end{pmatrix} w(t), \tag{A5}$$

$$y(t) = (1\ 0) \begin{pmatrix} v'_{\text{tip}} \\ x_{\text{tip}} \end{pmatrix} - u(t) + v(t), \tag{A6}$$

where an altered form of the tip velocity $v'_{\text{tip}} = v_{\text{tip}} - (\omega_n/Q)x_{\text{base}}$ is introduced.

According to the separation principle,[25] the problem of finding an optimal controller can be divided into the two subproblems of constructing an optimal regulator and an optimal estimator.

1. Optimal regulator

The steady-state optimal control $\mathbf{u}(t)$ for a given state $\mathbf{x}(t)$ is generated by the control law,

$$\mathbf{u}(t) = -\mathbf{K}\mathbf{x}(t), \tag{A7}$$

where the Kalman gain matrix is given by $\mathbf{K} = \mathbf{R_c}^{-1}\mathbf{B}^{\mathbf{T}}\mathbf{S}$, with $\mathbf{S}$ (a symmetric 2×2 matrix) as the solution of the steady-state Riccati equation,

$$0 = \mathbf{S}\mathbf{A} + \mathbf{A}^{\mathbf{T}}\mathbf{S} - \mathbf{S}\mathbf{B}\mathbf{R_c}^{-1}\mathbf{B}^{\mathbf{T}}\mathbf{S} + \mathbf{Q_c}. \tag{A8}$$

A suitable choice for the weighing matrices $\mathbf{Q_c}$ and $\mathbf{R_c}$ are the maximum variances in the tip and base displacements, $\sigma^2_{x,\text{tip}}$ and $\sigma^2_{x,\text{base}}$, respectively,[8]

$$\mathbf{Q_c} = \begin{pmatrix} 0 & 0 \\ 0 & 1/\sigma^2_{x,\text{tip}} \end{pmatrix} \quad \text{and} \quad \mathbf{R_c} = 1/\sigma^2_{x,\text{base}}. \tag{A9}$$

The analytical expression for $\mathbf{K}$ is obtained by solving the three independent equations contained in (A8) (cf. Ref. 26, p. 347 for an example),

$$\mathbf{K} = \left(\frac{\alpha}{\omega_n}, \frac{\alpha}{Q} + \frac{\alpha^2/2 + \alpha/Q}{1 - \alpha/Q} \right), \tag{A10}$$

where α is given by (13).

The closed-loop properties are found by inspecting the characteristic equation,

$$|s\mathbf{I} - \mathbf{A} + \mathbf{B}\mathbf{K}| = 0, \tag{A11}$$

from which the closed-loop frequency ω_{cl} and quality Q_{cl} can be determined,

$$\omega_{\text{cl}} = \omega_n \sqrt{\frac{1 + \alpha^2/2}{1 - \alpha/Q}}, \tag{A12}$$

$$Q_{\text{cl}} = Q \frac{\sqrt{(1 + \alpha^2/2)(1 - \alpha/Q)}}{1 + \alpha Q - \alpha^2/2}. \tag{A13}$$

2. Optimal observer

The optimal observer is needed to reconstruct the actual state $\hat{\mathbf{x}}(t)$ from the incomplete information provided by the measured system output $\mathbf{y}(t)$. "Optimal" means that the deviation of $\hat{\mathbf{x}}(t)$ from the exact state $\mathbf{x}(t)$ is minimized. Given the differential equation defining the reconstructed state,

$$\dot{\hat{\mathbf{x}}} = \mathbf{A}\hat{\mathbf{x}} + \mathbf{B}\mathbf{u} + \mathbf{L}(\mathbf{y} - \mathbf{C}\hat{\mathbf{x}} - \mathbf{D}\mathbf{u}). \tag{A14}$$

The deviation is smallest if the gain matrix $\mathbf{L}$ is selected according to $\mathbf{L} = \mathbf{P}\mathbf{C}^{\mathbf{T}}\mathbf{R_e}^{-1}$ (Kalman-Bucy filter) as implied by the steady-state Riccati equation of the optimal estimator,

$$0 = \mathbf{A}\mathbf{P} + \mathbf{P}\mathbf{A}^{\mathbf{T}} - \mathbf{P}\mathbf{C}\mathbf{R_e}^{-1}\mathbf{C}^{\mathbf{T}}\mathbf{P} + \mathbf{G}\mathbf{Q_e}\mathbf{G}^{\mathbf{T}}. \tag{A15}$$

Here, the two noise variances $\mathbf{Q_e} = \sigma_w^2$ and $\mathbf{R_e} = \sigma_v^2$ represent the amount of the excitation and measurement noise present. Solving for $\mathbf{P}$ (which is also a symmetric 2×2 matrix) simi-

larly to the optimal regulator problem, the optimal gain matrix is obtained,

$$\mathbf{L} = \begin{pmatrix} \beta^2 \omega_n^2/2 \\ \beta \omega_n \end{pmatrix}, \tag{A16}$$

where β is given by (14). A closer look at Eq. (A15) reveals that the observer is independent of the control force $\mathbf{u}$; consequently the choice of the beam deflection detection scheme [manifested by the appearance of the control term in the detection, Eq. (A6)] has no influence on the gain matrix $\mathbf{L}$.

3. Optimal controller

The stochastic optimal controller is obtained by combining optimal regulator and estimator. Substituting $\mathbf{u}(t)$ in (A14) by (A7), the optimal controller is determined by

$$\dot{\hat{\mathbf{x}}} = \mathbf{A}\hat{\mathbf{x}} - \mathbf{B}\mathbf{K}\hat{\mathbf{x}} + \mathbf{L}(\mathbf{y} - \mathbf{C}\hat{\mathbf{x}} + \mathbf{D}\mathbf{K}\hat{\mathbf{x}}). \tag{A17}$$

In terms of transfer functions, the controller is given as the ratio of the Laplace transforms $U(s)$ and $Y(s)$ (the control and output variable), respectively,

$$H_{\mathrm{oc}}(s) = \frac{U(s)}{Y(s)} = \frac{X_{\mathrm{base}}(s)}{X_{\mathrm{PSD}}(s)} = \mathbf{K}(s\mathbf{I} - \mathbf{A_c})^{-1}\mathbf{L}, \tag{A18}$$

where $\mathbf{A_c} = \mathbf{A} - \mathbf{B}\mathbf{K} - \mathbf{L}\mathbf{C} + \mathbf{L}\mathbf{D}\mathbf{K}$. Considering Eq. (8), the "standard form" of $H_{\mathrm{oc}}(s)$, the controller parameters can be identified with

$$K_{\mathrm{oc}} = \mathbf{K}\mathbf{L}, \tag{A19}$$

$$z_{\mathrm{oc}} = \frac{\mathbf{K}\ \mathrm{adj}(\mathbf{A}_c)\mathbf{L}}{\mathbf{K}\mathbf{L}}, \tag{A20}$$

$$\omega_{\mathrm{oc}} = \sqrt{\det(\mathbf{A_c})}, \tag{A21}$$

$$Q_{\mathrm{oc}} = \omega_{\mathrm{oc}}/\mathrm{Tr}(\mathbf{A_c}), \tag{A22}$$

and using matrix adjugate of $\mathbf{A_c}$, determinant, and trace.[27] Substituting $\mathbf{K}$, $\mathbf{L}$, and $\mathbf{A_c}$ then produces the explicit expressions (9)–(12).

The general result (A18) can be adapted for other actuation/detection schemes. For interferometer detection using base actuation, the measured system output is equivalent to tip position $y(t) = x_{\mathrm{tip}}(t)$, hence $\mathbf{A_c} = \mathbf{A} - \mathbf{B}\mathbf{K} - \mathbf{L}\mathbf{C}$. For tip actuation, the same substitution applies (for both detection schemes), and furthermore the Kalman gain $\mathbf{K}$ must be replaced by[8]

$$\mathbf{K} = \left(\frac{\alpha}{\omega_n}, \frac{\alpha}{Q} + \frac{\alpha^2}{2} \right), \tag{A23}$$

with a modified α,

$$\alpha = \sqrt{\frac{1}{Q^2} + 2\zeta_c - 2} - \frac{1}{Q} \text{ and } \zeta_c^2 = 1 + \frac{\sigma_{x,\mathrm{tip}}^2}{\sigma_{x,\mathrm{base}}^2}. \tag{A24}$$

[1] T. R. Albrecht, P. Grütter, D. Horne, and D. Rugar, J. Appl. Phys. **69**, 668 (1991).
[2] J. Mertz, O. Marti, and J. Mlynek, Appl. Phys. Lett. **62**, 2344 (1993).
[3] U. Dürig, H. R. Steinauer, and N. Blanc, J. Appl. Phys. **82**, 3641 (1997).
[4] D. Rugar, C. S. Yannoni, and J. A. Sidles, Nature (London) **360**, 563 (1992).
[5] J. A. Sidles, J. L. Garbini, K. J. Bruland, D. Rugar, O. Züger, S. Hoen, and C. S. Yannoni, Rev. Mod. Phys. **67**, 249 (1995).
[6] T. D. Stowe, K. Yasumura, T. W. Kerry, D. Botkin, K. Wago, and D. Rugar, Appl. Phys. Lett. **71**, 288 (1997).
[7] D. Rugar, R. Budakian, H. J. Mamin, and B. W. Chui, Nature (London) **430**, 329 (2004).
[8] J. L. Garbini, K. J. Bruland, W. M. Dougherty, and J. A. Sidles, J. Appl. Phys. **80**, 1951 (1996).
[9] K. J. Bruland, J. L. Garbini, W. M. Dougherty, and J. A. Sidles, J. Appl. Phys. **80**, 1959 (1996).
[10] Ch. Loppacher *et al.*, Appl. Phys. A: Mater. Sci. Process. **66**, 215 (1998).
[11] B. Friedland, *Advanced Control System Design* (Prentice Hall, New Jersey, 1996), p. 233.
[12] S. Chao, W. M. Dougherty, J. L. Garbini, and J. A. Sidles, Rev. Sci. Instrum. **75**, 1175 (2004).
[13] D. Rugar and P. Grütter, Phys. Rev. Lett. **67**, 699 (1991).
[14] G. Meyer and N. M. Amer, Appl. Phys. Lett. **53**, 2400 (1988).
[15] The relation between x_{base} and f depends on the actual damping mechanism. When working in vacuum internal friction is usually dominating and $f/k = x_{\mathrm{base}} + \dot{x}_{\mathrm{base}}/\omega_n Q$. For air damping $f/k = x_{\mathrm{base}}$.
[16] D. Sarid, *Scanning Force Microscopy* (Oxford University Press, New York, 1991), p. 119.
[17] G. F. Franklin, J. D. Powell, and M. L. Workman, *Digital Control of Dynamic Systems* (Addison Wesley, Menlo Park, CA, 1998), p. 73.
[18] R. Saucedo and E. E. Schiring, *Introduction to continuous and digital control systems* (The Macmillan Company, New York, 1968), p. 103.
[19] See, e.g., the control systems toolbox of MATLAB.
[20] *Advanced Control System Design* (Ref. 11), p. 219.
[21] As a rule of thumb, the fastest process should be within $\approx 1/30$ of the controller bandwidth, given as half the sampling rate (Ref. 17).
[22] C. L. Degen, Q. Lin, A. Hunkeler, U. Meier, M. Tomaselli, and B. H. Meier, Phys. Rev. Lett. **94**, 207601 (2005).
[23] G. Moresi, Ph.D. thesis, Universitat Basel, Switzerland, 2005.
[24] B. C. Stipe, H. J. Mamin, T. D. Stowe, T. W. Kenny, and D. Rugar, Phys. Rev. Lett. **87**, 096801 (2001).
[25] H. Kwakernaak and R. Sivan, *Linear Optimal Control Systems* (Wiley, New York, 1972).
[26] B. Friedland, *Control System Design: An Introduction to State-Space Methods* (McGraw-Hill, New York, 1986).
[27] The adjugate of the 2×2 matrix $\mathbf{M} = \left(\begin{smallmatrix} m_{11} & m_{12} \\ m_{21} & m_{22} \end{smallmatrix}\right)$ is given by $\mathrm{adj}(\mathbf{M}) = \mathbf{M}^{-1} \det(\mathbf{M}) = \left(\begin{smallmatrix} m_{22} & -m_{12} \\ -m_{21} & m_{11} \end{smallmatrix}\right)$.